Mechanisms of B-Cell Synapse Formation Predicted by Monte Carlo Simulation

Philippos K. Tsourkas,* Nicole Baumgarth,† Scott I. Simon,* and Subhadip Raychaudhuri*
*Department of Biomedical Engineering, and †Center for Comparative Medicine, University of California-Davis, Davis, California

ABSTRACT The clustering of B-cell receptor (BCR) molecules and the formation of the protein segregation structure known as the ''immunological synapse'' at the contact region between B cells and antigen presenting cells appears to precede antigen (Ag) uptake by B cells. The mature B-cell synapse is characterized by a central cluster of BCR/Ag molecular complexes surrounded by a ring of LFA-1/ICAM-1 complexes. In this study, we investigate the biophysical mechanisms that drive immunological synapse formation in B cells by means of Monte Carlo simulation. Our approach simulates individual reaction and diffusion events on cell surfaces in a probabilistic manner with a clearly defined mapping between our model's probabilistic parameters and their physical equivalents. Our model incorporates the bivalent nature of the BCR as well as changes in membrane shape due to receptor-ligand binding. We find that differences in affinity and bond stiffness between BCR/Ag and LFA-1/ICAM-1 are sufficient to drive synapse formation in the absence of membrane deformation. When significant membrane deformation occurs as a result of receptor-ligand binding, our model predicts the affinity-dependent mechanism needs to be complemented by a BCR signaling-driven shift in LFA-1 affinity from low to high in order for synapses to form.

INTRODUCTION

Specific recognition of foreign antigens by lymphocytes is central to the adaptive immune response. However, precisely how lymphocytes differentially respond to antigenic stimuli of varying type and strength remains unknown. Recent experimental evidence suggests antigen (or MHC-loaded peptides for the T-cell/APC system) presentation on the restricted geometry of a two-dimensional cell surface, together with recruitment of antigen into segregated clusters of receptor-ligand complexes, could be one possible mechanism by which lymphocytes recognize and respond to antigen (1–9).

The clustering of receptor molecules on the cell surface and the formation of segregated protein structures increasingly is seen as an efficient mechanism of cellular information exchange during cell-cell interactions (10). In the immune system, such clustering and segregation of membrane-bound proteins is observed at the intercellular junction between lymphocytes and antigen presenting cells (APC) as they become adherent and engage in antigen recognition. Because of the resemblance to neurological synapses, these structures have been collectively termed ''immunological synapses'' (2–4).

The mature B-cell synapse consists of a central cluster of B-cell receptor/antigen (BCR/Ag) molecular complexes (sometimes also referred to as the central supramolecular activation cluster, or c-SMAC), surrounded by a ring of lymphocyte function-associated antigen-1/intercellular adhesion molecule-1 (LFA-1/ICAM-1) complexes (also known as the peripheral SMAC, or p-SMAC). This is the much-studied canonical form of the immune synapse first observed at the intercellular junction between a T cell and an APC (1–4).

Although the mechanisms that drive synapse formation in T cells have extensively been modeled (11–18) since the pioneering work of Qi et al. (11), less is known about the mechanisms that govern synapse formation in B cells. Even though the structure of the B-cell synapse is similar to that of the canonical form of the T-cell synapse, factors such as receptor affinity, density, shape, and extracellular domain length vary significantly between T cells and B cells. B-cell receptors (BCRs) are bivalent antibody molecules (IgM and IgD for naïve B cells) whereas T-cell receptors are monovalent. Moreover, the affinity of BCR for antigen can vary between 10^5 M^{-1}–10^{10} M^{-1}, as compared to 10^4 M^{-1}–10^7 M^{-1} in the case of T-cell receptors (TCRs) for MHCp. Furthermore, the typical density of BCR on B-cell surfaces ($\sim$200 molecules/μm^2) is an order of magnitude greater than the typical density of TCR on a T-cell surface ($\sim$20 molecules/μm^2). Importantly, the extracellular domain length of BCR/Ag complexes in B-cell synapse experiments (5–7) is close to that of LFA-1/ICAM-1 complexes ($\sim$40 nm), which is markedly different from that of TCR/MHCp complexes ($\sim$15 nm). The relatively short length of TCR/MHCp bonds is considered to be one of the major driving factors in T-cell synapse formation (11). For these reasons, it is thought that the mechanisms that drive synapse formation in B cells differ substantially from those in T cells (19).

B-cell synapse formation might be driven by signaling that results in changes in membrane shape as a result of affinity-dependent BCR/Ag binding (8). Alternatively, B-cell receptor clustering in B cells defective in signaling might be explained by the so-called ''diffusion and binding'' hypothesis (19). According to the latter model, the synapse forms mainly by undirected diffusion of receptors into the contact zone, whereupon they bind with high affinity and stay in

Submitted August 10, 2006, and accepted for publication February 5, 2007.
Address reprint requests to Subhadip Raychaudhuri, E-mail: raychaudhuri@ucdavis.edu.

0006-3495/07/06/4196/13 $2.00
doi: 10.1529/biophysj.106.094995

place or are eventually expelled by crowding at the center of the contact zone. The experimental work (19) on which this model was based upon has crucial limitations, however, in that only a limited range of affinity ($K_A \sim 10^8$–10^{10} M^{-1}) was considered, despite the fact that B cells can recognize antigen over $K_A \sim 10^6$–10^{10} M^{-1}. In addition, the model does not consider the formation of the surrounding ring of LFA-1/ICAM-1 complexes observed in B-cell synapse experiments (5–7).

In this study, we investigate the molecular mechanisms of that drive B-cell synapse formation by systematically studying the effect of biophysical parameters. Our approach consists of a stochastic, agent-based computer model of B-cell/APC interaction in which individual molecular events such as diffusion and reaction are simulated using probabilistic rules. Individual parameter values can be varied in a controlled manner in successive in silico experiments to identify their contribution, or negate their importance, to the process of synapse formation. Interestingly, we are able to clearly define a mapping between the probabilistic parameters used in our simulation and their experimentally measured counterparts. Such a mapping scheme is crucial if we are to compare the results of in silico simulations to those of immunological experiments (20).

Our results show that differences in affinity and bond stiffness between BCR/Ag and LFA-1/ICAM-1 are sufficient to account for synapse formation when the affinity of BCR for antigen is less than that of LFA-1 for ICAM-1 and in the absence of membrane deformation (as is the case at the onset of synapse formation). For high-affinity BCR/Ag binding, our model predicts that it is necessary for BCR/Ag bonds to be stiffer than LFA-1/ICAM-1 bonds for a synapse to form. However, when significant membrane deformation is allowed in our model, active, signaling driven processes become necessary for synapse formation. One example of such a signaling-driven process is a shift in the affinity of LFA-1 from an initial low affinity state to a high-affinity state as a result of BCR signaling (6,7,9).

MODEL

Background

A Monte Carlo method was applied to model B-cell synapse formation. Thus, the molecular population is randomly sampled to undergo events such as diffusion and reaction, with its status updated at every time step. Monte Carlo methods have been successfully employed in the past to understand immune cell receptor-ligand binding, clustering, and signaling (13,18,20–24). Our model's distinguishing features are: i), the use of probabilistic rate constants instead of an energy-based Metropolis algorithm; ii), explicit spatial simulation of molecules; and iii), treatment of diffusion of receptor-ligand complexes. The explicit spatial simulation of molecules allows the modeling of crowding and exclusion effects that are potentially important in synapse formation but cannot easily be captured by differential equation-based models, particularly if more than one molecular species is present. The discrete nature of our model also eliminates the need to make assumptions about the continuity of molecular concentrations, which may not be valid at low antigen concentration. This is particularly relevant in light of the fact that antigen concentration is usually low at the onset of an immune response.

Model setup

As shown in Fig. 1, the section of the B-cell/APC system we wish to model is the region of closest approach between the

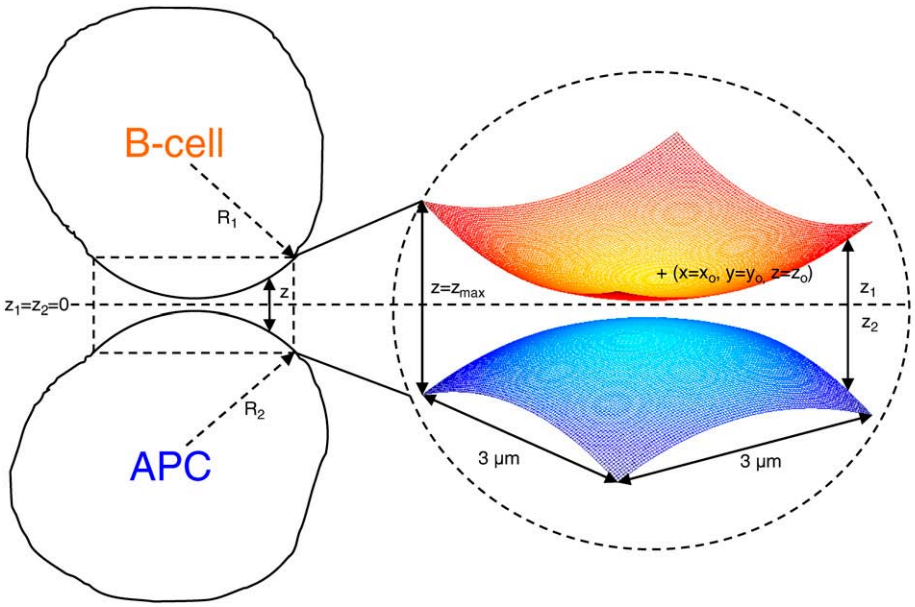

FIGURE 1 Model of the B-cell/APC contact region. The cells are assumed to have a spherical shape, with the total vertical separation distance between the two surfaces at any point $z = z_1 + z_2$, with z_1 and z_2 given by Eq. 1. At the center of the contact zone (x_o, y_o), the vertical separation distance is at its minimum $z = z_o$, whereas at the corners it is $z = z_{max}$. The 3 μm $\times$ 3 μm simulated area is large enough to include the entire zone where binding is possible.

two cells, where the distance between the membranes is small enough to allow binding between molecules on opposite surfaces. The cell membranes are modeled as two Cartesian lattices, each discretized in an *NXN* grid of nodes. We assume the membranes initially have a spherical curvature, which, in the absence of external forces, both cells would tend toward to minimize surface energy. The total vertical separation distance z between the two surfaces at any given point (x, y) is given by $z = z_1 + z_2$, as in Fig. 1, with the half-heights z_1 and z_2 each given by:

$$z_i(x,y) = \frac{z_o}{2} + R_i - \left(R_i^2 - \left((x-x_0)^2 + (y-y_0)^2\right)\right)^{1/2}. \quad (1)$$

At the center of the contact zone ($x = x_o$, $y = y_o$), the vertical separation between the two surfaces is at its minimum value, $z = z_o$. We also can simulate a cell-bilayer system such as the one used in many synapse experiments (6–8) in the limit as $R_2 \rightarrow \infty$ and $z_2(x,y) \rightarrow z_o/2$.

The size of the region we have chosen to simulate in our model is 3 μm $\times$ 3 μm, which is large enough to include the entire region over which binding can occur for spherical curvature (see Fig. 2), and also larger than typical experimentally observed synapse diameters of ~2 μm (6,7). In addition, this area is believed to be sufficiently large such that a zero net flux condition exists at the boundaries, which in our agent-based simulator is simulated by means of fully reflecting boundaries. Only one molecule can occupy a node in our simulation, so we choose a nodal spacing equal to a membrane protein molecule's exclusion radius, ~10 nm (resulting in 300 $\times$ 300 nodes). The exception are BCR molecules, which being bivalent, have a width of ~25 nm (25,26), and thus occupy three nodes, with either a horizontal or vertical orientation on the lattice. The various parameters that relate to the spatial dimensions of our model are listed in Table 1.

Simulation procedure: reaction and diffusion "moves"

At the start of a simulation run, molecules are uniformly distributed over the two surfaces at random. The molecular species represented are BCR and LFA-1 on the B-cell surface and antigen and ICAM-1 on the APC or bilayer surface. At every time step in the simulation, molecules from the population are individually sampled at random to attempt either diffusion or reaction events, determined by means of a coin toss with probability 0.5.

Reaction

If a molecule has been selected to undergo a reaction, the first step is to check the same node on the opposite surface for a complementary molecule. If that is the case, a random number trial with probability $p_{on(i)}$ is performed to determine if the two molecules will bind together and form a molecular

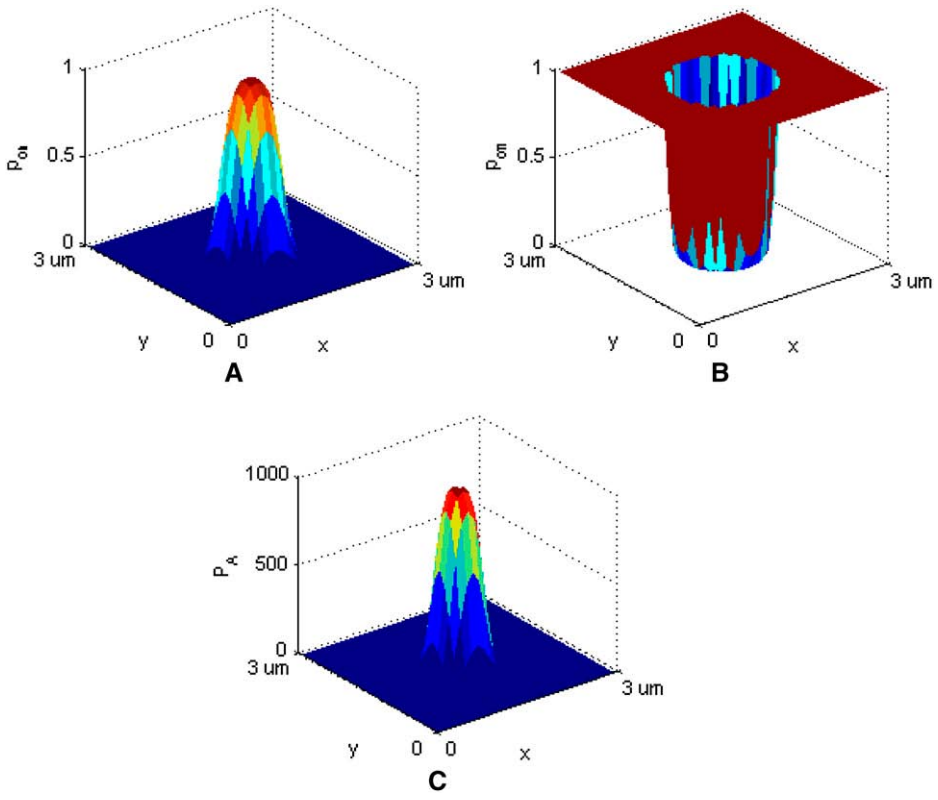

FIGURE 2 Sample graphical representation of (*A*) p_{on}, (*B*) p_{off}, and (*C*) P_A according to Eqs. 2–4. Receptor-ligand binding can only occur where $p_{on} > 0$ and $p_{off} < 1$. In this set of images, $\kappa' = 40$ μN/m, $\kappa = 2\kappa'$, $z_{eq} =$ 42 nm, $k_B = 1.38 \times 10^{-23}$ J/K, $T = 300$ K, $p_{on} = 1.0$ and $p_{off} = 0.001$.

TABLE 1 Spatial dimensions of the model

Parameter	Value
Size of contact region	3 μm × 3 μm
Number of nodes	300 × 300
Nodal spacing	10 nm
Cell radius (B Cell, APC)	6 μm
z_{max} from Eq. 1 (cell-bilayer case)	390 nm + z_o

complex. BCR molecules are modeled as being bivalent and occupy three nodes while being able to bind up to two antigen molecules, one on each end node (but not the middle node). If a free BCR molecule is selected for a reaction, a coin toss is additionally performed to pick one of the end nodes, and the APC surface opposite the chosen node is checked for a free antigen molecule. Sometimes a BCR molecule may have bound an antigen molecule on one Fab domain and have the other Fab domain free, forming a BCR/Ag complex. If the free Fab domain is selected, the reaction proceeds as described above, which may result in a second antigen molecule binding to the BCR/Ag complex (forming a BCR/Ag_2 complex), while if the Fab domain with the bound antigen is selected, the BCR/Ag complex may dissociate into its component molecules with probability $p_{off(i)}$. If a BCR/Ag_2 molecule is selected, one of the two Fab domains is selected at random to undergo dissociation as described above, resulting in the formation of a BCR/Ag complex and a free antigen molecule. Three reversible reactions are possible: LFA-1+ICAM-1 ↔ LFA-1/ICAM-1, BCR+Ag ↔ BCR/Ag, and BCR/Ag+Ag ↔ BCR/Ag_2. The binding and dissociation probabilities for the two reactions involving BCR are assumed to be the same and thus the subscript i refers to the BCR/Ag reactions when $i = BA$ and the LFA-1/ICAM-1 reaction when $i = LI$.

We assume the probability of bond formation depends on the intermembrane distance z in accordance to the well-known linear spring model (27,28). Replacing the rate constant k_{on} with the probability p_{on}, we obtain the following probability density function:

$$p_{on(i)}(z) = p_{on(i)}^{max}\exp\left(-\frac{\kappa_i'(z - z_{eq(i)})^2}{2k_BT}\right). \quad (2)$$

The bond is modeled as a mechanical spring with stiffness κ' and equilibrium length z_{eq}, whereas k_B denotes the Boltzmann constant (1.38×10^{-23} J/K) and T the temperature (~300 K). The probability of binding is greatest at the point $z(x,y) = z_{eq}$, which will be the center of contact zone when $z_{eq} = z_o$, as in Fig. 2 *A*. In formulating our model, we assumed that as the two cells move closer to one another and z_o decreases, the first binding event is likely to occur when z_o approaches the value of z_{eq} of one of the species, after which the cells stop moving toward each other. In our simulations we thus set z_o equal to either $z_{eq(BA)}$ or $z_{eq(LI)}$, depending on the circumstances.

Similarly, the dissociation probability $p_{off(i)}$ is given by (27,28):

$$p_{off(i)}(z) = p_{off(i)}^{min}\exp\left(\frac{(\kappa_i - \kappa_i')(z - z_{eq(i)})^2}{2k_BT}\right). \quad (3)$$

Without loss of generality, we can set $\kappa_{(i)} = 2\kappa'_{(i)}$ so that the exponential in Eq. 3 is the same as that in Eq. 2 but with a positive sign in front. In contrast to p_{on}, p_{off} is a minimum at $z = z_{eq}$, increasing away from this point, as in Fig. 2 *B*, where we also see that p_{off} cannot exceed 1.0.

Since p_{on} and p_{off} are analogous to k_{on} and k_{off}, we can obtain the probabilistic analog to the association constant K_A, denoted as P_A, by dividing Eq. 2 by Eq. 3 and setting $\kappa_{(i)} = 2\kappa'_{(i)}$:

$$P_{A(i)}(z) = \frac{p_{on(i)}^{max}}{p_{off(i)}^{min}}\exp\left(-\frac{(\kappa_i(z - z_{eq(i)})^2}{2k_BT}\right) = P_{A(i)}^{max}\exp\left(-\frac{\kappa_i(z - z_{eq(i)})^2}{2k_BT}\right). \quad (4)$$

A typical plot of $P_{A(i)}(z)$ is shown in Fig. 2 *C*. The height of the peak is determined by the intrinsic affinity of the receptor-ligand pair, $P_{A(i)}^{max}$, whereas the bond stiffness κ_i determines how far from the optimum intermembrane spacing bonds can form, and hence the width of the peak in Fig. 2 *C*. The quantity $P_{A(i)}(z)$ defined in Eq. 4 thus denotes the overall receptor-ligand affinity, which consists of both the intrinsic affinity and the bond stiffness. Individually varying p_{on}^{max} and p_{off}^{min} while keeping the ratio P_A^{max} constant changes the timescale of the simulation, but not the equilibrium behavior. It is important to note that $P_A(z)$ is not a probability but a probability ratio. The intrinsic affinity P_A^{max} most closely corresponds to the quantity K_A and the mapping between K_A, k_{on}, k_{off}, and P_A^{max}, p_{on}^{max}, p_{off}^{min}, respectively, is given in the Appendix.

Diffusion

On the other hand, if a molecule has been selected to undergo diffusion, a random number trial with probability $p_{diff(i)}$ is used to determine if the diffusion move will occur successfully. If the trial is successful, the selected molecule will ''hop'' by a distance of one nodal spacing in one of four possible directions with equal probability. Because molecules are not allowed to occupy the same node, the diffusion hop will only occur if the appropriate nodes are unoccupied. For example, three nodes need to be free for a BCR molecule to diffuse the direction transverse to its length, whereas only one free node is needed in order for it to diffuse along its length. In the case of complexes, the appropriate nodes on both surfaces need to be free (two nodes for monomeric LFA-1/ICAM-1 complexes, two or four for BCR/Ag complexes, and three or five for BCR/Ag_2 complexes). The mapping between $p_{diff(i)}$ and the diffusion coefficient D is given in the Appendix.

Membrane free energy and deformation

Our simulation also allows the modeling of changes in the originally spherical membrane shape as a result of receptor-ligand binding. We use the membrane free energy used by Qi et al. (11) and Weikl and Lipowsky (18), which has the following form:

$$E = \frac{1}{2}\iint \left[\kappa_{BA} C_{BA}\left(z - z_{eq(BA)}\right)^2 + \kappa_{LI} C_{LI}\left(z - z_{eq(LI)}\right)^2\right] dxdy + \frac{1}{2}\iint \left[\gamma(\nabla z)^2 + \beta(\nabla^2 z)^2\right] dxdy. \quad (5)$$

The first integral in the equation relates to the energy associated with receptor-ligand bond stretching, which is a function of the concentration of BCR/Ag and BCR/Ag_2 complexes, C_{BA}, and the concentration of LFA-1/ICAM-1 complexes, C_{LI}, whereas the other two terms relate to the energy associated with membrane tension (γ) and bending rigidity (β), respectively. The change in the membrane separation distance z is modeled according to the well-known Landau-Ginzburg formulation in the manner of Qi et al. (11), which for the geometry used here has the form:

$$\frac{\partial z}{\partial t} = M\left(-\kappa_{BA} C_{BA}\left(z - z_{eq(BA)}\right) - \kappa_{LI} C_{LI}\left(z - z_{eq(LI)}\right) + \gamma\nabla^2 z - \beta\nabla^4 z\right). \quad (6)$$

The constant M relates the timescale of membrane deformation relative to that of receptor-ligand binding, such that for small M, the membrane will essentially retain its shape for the duration of the simulation. Because the length scale of membrane deformation (set by $(\beta/\gamma)^{1/2}$) is considerably larger than that of a protein's exclusion radius (~100 nm instead of ~10 nm), for the purpose of calculating z we coarse-grain the NXN membrane surface lattice into 10×10 node subdomains over which z is constant. The concentration of BCR/Ag, BCR/Ag_2 and LFA-1/ICAM-1 complexes in each of these subdomains is then calculated and entered in the discrete form of Eq. 6.

Monte Carlo time step

In our algorithm, a number S of diffusion/reaction trials is performed during every time step, at the end of which the membrane height is adjusted using Eq. 6 with Dirichlet boundary conditions obtained from Eq. 1. The number of trials S is set equal to the total number of molecules (free and complexes) present in the system at the beginning of each time step, and the simulation is run for a number of time steps T. Each Monte Carlo time step corresponds to 10^{-3} s, as shown in the Appendix. A summary of our Monte Carlo algorithm is shown in Fig. 3.

Model parameters

Our investigation strategy consists of successive virtual experiments in which individual parameter values are varied

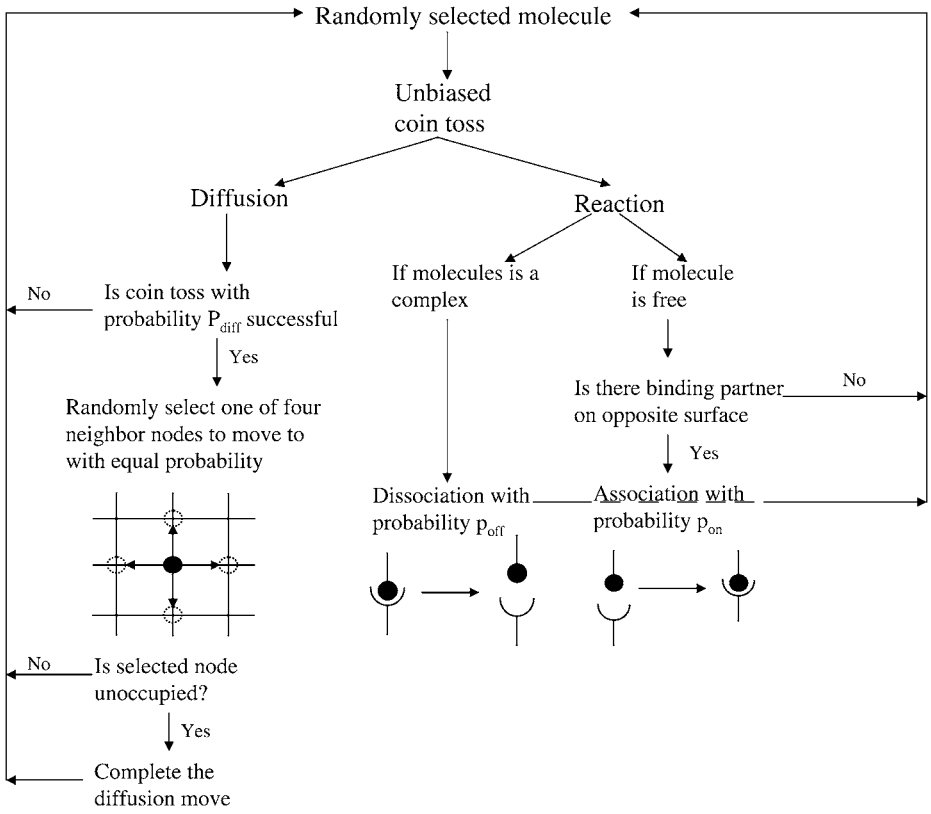

FIGURE 3 Monte Carlo algorithm flow chart.

to determine the role of each parameter on synapse formation. Table 2 lists all biological parameters whose values can be varied in our simulations, excluding the spatial parameters listed in Table 1.

Many of the model parameters in Table 2 do not appear to vary significantly during physical experiments. Relevant experimentally obtained parameter values are listed in the two columns on the left-hand side of Table 3. In some cases, it is necessary to map the experimental value into the probabilistic analogs used by our model (see Appendix), as is the case with K_A, k_{on}, k_{off} and P_A^{max}, p_{on}^{max}, p_{off}^{min}, respectively. Adapted forms of the experimentally-derived published parameter values used in our simulations are listed in the two columns on the right-hand side of Table 3.

Diffusion coefficients of free molecules in a biological membrane are in the range of ~0.01–0.1 $\mu m^2/s$ (30), with little variation between species. We thus collectively group the individual diffusion probabilities of the free molecule species from Table 2 ($p_{diff(B)}$, $p_{diff(A)}$, $p_{diff(L)}$, $p_{diff(I)}$) into a single parameter $p_{diff(F)}$, and likewise group the individual diffusion probabilities of the complexes, $p_{diff(BA)}$ and $p_{diff(LI)}$, into a single parameter $p_{diff(C)}$. A diffusion coefficient of the order of 0.1 $\mu m^2/s$ approximately corresponds to $p_{diff(F)} = 1.0$ (see Appendix), while $p_{diff(C)}$ is assumed to be unknown and therefore variable.

The number of variable parameters can be further reduced by making assumptions regarding the number of free BCR and LFA-1 molecules initially present on the B-cell surface, B_0 and L_0. For instance, assuming a typical membrane protein molecule distribution of 10^5 molecules/cell (12,31), and using a typical lymphocyte radius of 6 μm (resultant area ~450 μm^2), the average molecular density is ~220 molecules/μm^2. For a contact area of 9 μm^2, this means $B_0 = L_0 = 2000$. Because we are assuming a zero flux condition at the boundaries, the number of free molecules (B_0, L_0, A_0, I_0) cannot increase above this initial value. Binding and clustering at the center of the contact zone, however, will result in a concentration gradient that in real situations would cause a net flux of molecules into the contact zone. To address this, we compensate by setting the initial number of free molecule to a value higher than that given in experiments (6). From our simulations, we find that the number of complexes formed is not too large compared to B_0, L_0, A_0, and I_0 (of the order of hundreds) and we thus set $B_0 = L_0 = 3000$, which is sufficient to compensate for diffusion into the contact zone. A similar approach is used for I_0 and A_0.

TABLE 2 Parameters of the model

Parameter	Description
$p_{on(BA)}^{max}$	Maximum BCR/Ag, BCR/Ag_2 complex formation probability
$p_{off(BA)}^{min}$	Minimum BCR/Ag, BCR/Ag_2 complex dissociation probability
$p_{on(LI)}^{max}$	Maximum LFA-1/ICAM-1 complex formation probability
$p_{off(LI)}^{min}$	Minimum LFA-1/ICAM-1 complex dissociation probability
B_0	Initial number of free BCR molecules
A_0	Initial number of free antigen molecules
L_0	Initial number of free LFA-1 molecules
I_0	Initial number of free ICAM-1 molecules
κ_{BA}	Stiffness of BCR/Ag bond
κ_{LI}	Stiffness of LFA-1/ICAM-1 bond
$z_{eq(BA)}$	Equilibrium extracellular length of BCR/Ag complex
$z_{eq(LI)}$	Equilibrium extracellular length of LFA-1/ICAM-1 complex
$p_{diff(B)}$	Probability of diffusion of a free BCR molecule
$p_{diff(A)}$	Probability of diffusion of a free antigen molecule
$p_{diff(L)}$	Probability of diffusion of a free LFA-1 molecule
$p_{diff(I)}$	Probability of diffusion of a free ICAM-1 molecule
$p_{diff(BA)}$	Probability of diffusion of a BCR/Ag, BCR/Ag_2 complex
$p_{diff(LI)}$	Probability of diffusion of a LFA-1/ICAM-1 complex
M	Timescale of membrane deformation
γ	Membrane tension
β	Membrane bending rigidity

It also is possible to estimate the equilibrium extracellular domain length of the BCR/Ag complex, even though an exact number is not available in the literature. In the in vitro experiments we are basing our model on, the antigen molecules are part of antigen-antibody immune complexes loaded onto Fc receptors (5–8), which would indicate a minimum extracellular domain length comparable to that of LFA-1/ICAM-1 complexes, i.e., ~42 nm. However, it also is possible that in certain in vivo situations the antigens on the APC surface are fragments <1 nm in length, which would set the lower bound on the length of BCR/Ag complexes to the typical length of an antibody molecule, 22–23 nm (25,26). In our investigation we thus perform experiments where the length of the BCR/Ag complexes is set to either 22 or 42 nm.

When these assumptions and simplifications have been entered into our model, the list of variable parameters reduces to that shown in Table 4. These are the parameters for which defined values have not been reported, such as κ_{BA} and $z_{eq(BA)}$, (and which may well vary), or those that are varied in actual synapse experiments, such as antigen molecule number A_0 and BCR affinity $P_{A(BA)}^{max} = p_{on(BA)}^{max}/p_{off(BA)}^{min}$. These also are therefore the parameters we focused on as possible driving factors of B-cell synapse formation.

RESULTS

No membrane deformation

Intrinsic affinity differences between BCR and LFA-1 can drive synapse formation at low BCR affinity

In nature, BCR affinity for antigen is critical in determining the strength of the B-cell response (32–36). In our simulations, we found that intrinsic BCR affinity can be a leading driver of synapse formation. In Fig. 4, the affinity of BCR for antigen is varied across four orders of magnitude, from $K_A = 10^5$–10^8 M^{-1}, whereas the affinity of LFA-1 for ICAM-1 is fixed at $K_A = 10^7$ M^{-1}. In Fig. 4 *A* ($K_A = 10^5$ M^{-1}), the affinity of BCR is clearly too low for a synapse to form, even though the traces of one are discernible. In Fig. 4 *B* ($K_A = 10^6$ M^{-1}), however, we can clearly see the difference in intrinsic affinity between BCR and LFA-1 is sufficient to produce patterns similar to experimentally observed B-cell

TABLE 3 Experimentally measured parameter values and their probabilistic counterparts

Experimental parameter	Measured value	Simulation parameter	Mapped value
K_A BCR/Ag	10^6–10^{10} M^{-1} (6,7)	$P^{max}_{A(BA)}$	10^2–10^6
k_{on} BCR/Ag	10^4–10^6 $M^{-1}s^{-1}$ (6,7)	$p^{max}_{on(BA)}$	0.001–0.1
k_{off} BCR/Ag	1–10^{-4} s^{-1} (6,7)	$p^{min}_{off(BA)}$	10^{-3}–10^{-7}
K_A LFA-1/ICAM-1	3.3 μm^2/molecules (29)	$P^{max}_{A(LI)}$	10^3
k_{on} LFA-1/ICAM-1	0.33 μm^2 s^{-1}/molecules (29)	$p^{max}_{on(LI)}$	0.1
k_{off} LFA-1/ICAM-1	0.1 s^{-1} (29)	$p^{min}_{off(LI)}$	10^{-4}
Antigen concentration	10–1000 molecules./μm^2 (6)	A_0	100–10,000 molecules
ICAM-1 concentration	170 molecules/μm^2 (6)	I_0	~2000 molecules
κ_{LI}	40 μN/m (12)	κ_{LI}	Same
$z_{eq(LI)}$	42 nm (12)	$z_{eq(LI)}$	Same
D free molecules	~0.1 μm^2/s (30)	$p_{diff(F)}$	1.0
γ	24 μN/m (12)	γ	Same
β	5×10^{-20} J (12)	β	Same

synapses (6–8). No such pattern is observed when the affinities are equal (Fig. 4 *C*), whereas an inverted pattern forms when BCR affinity exceeds LFA-1 affinity (Fig. 4 *D*). The patterns generated in Fig. 4 are stable over a timescale of hours, although they do not represent the final equilibrium state of the system. The time evolution and final equilibrium behavior of the patterns in Fig. 4 are discussed in the Supplementary Material.

Our explanation for this behavior is as follows: Initially, the various molecules, all in the free state, are scattered uniformly over the cell surfaces. Because the region where binding is possible (defined by $p_{on} > 0$ and $p_{off} < 1$ in Fig. 2) is relatively small compared to the overall region of contact, at the start of our simulations most molecules are located outside the region of binding. The synapse pattern forms as free molecules from the periphery randomly drift into the zone of binding until they eventually find a binding partner and form a complex. If the complexes have relatively low diffusivity, as is the case in Fig. 4, a ring-like pattern results as the complexes tend to stay near where they formed, at the edge of the region of binding. Over time these complexes may break up, and some of the newly freed molecules are equally likely to drift further into the zone of binding. As the probability of binding is higher and that of dissociation lower in the interior of the contact zone due to the curvature of the membrane, the ring-like pattern becomes more cluster-like over time. In Fig. 4 *B*, BCR has a lower affinity and higher k_{off} than LFA-1, so that it forms a cluster at a faster rate than LFA-1, thereby producing a synapse. The situation is reversed in Fig. 4 *D*, whereas a purely random pattern is produced in Fig. 4 *C* as the two species have the same affinity and off-rate. These results show that pattern formation is in large part driven by differences in intrinsic affinity between the BCR/Ag and LFA-1/ICAM-1 (and in particular k_{off}).

TABLE 4 Unknown or variable parameters

Parameter	Type
$p^{max}_{on(BA)}$	Known, variable
$p^{min}_{off(BA)}$	Known, variable
A_0	Known, variable
κ_{BA}	Unknown, may vary
$z_{eq(BA)}$	May vary between ~22 and 42 nm
M	Unknown
$p_{diff(C)}$	Unknown, may vary

BCR/Ag bond stiffness is crucial to synapse formation at high BCR affinity

It is clear from the above results that differences in intrinsic affinity between the two species are not sufficient to account for synapse formation across the entire physiological range of BCR affinity ($K_A = 10^6$–10^{10} M^{-1}). However, given there are several antibody molecules that serve as B-cell receptors, and that these receptors encounter a wide variety of antigens, it is reasonable to assume the stiffness of the BCR/Ag bond (κ_{BA}) will vary in addition to the intrinsic affinity. In our simulations we have discovered that increasing the stiffness of the BCR/Ag bond above that of the LFA-1/ICAM-1 bond can result in synapses forming over the entire physiological range of BCR affinity. For example, our simulations show that for BCR affinity $K_A = 10^8$ M^{-1} a synapse such as the one in Fig. 4 *B* will form with a BCR/Ag bond stiffness value of $\kappa_{BA} = 80$ μN/m, whereas an inverted synapse pattern formed when the bond stiffness of the two species was equal (Fig. 4 *D*). At higher BCR affinity values, a greater increase in BCR/Ag bond stiffness is necessary to produce a synapse ($\kappa_{BA} \approx 160$ μN/m at $K_A = 10^{10}$ M^{-1}).

Our explanation for this mechanism of synapse formation is that increasing bond stiffness narrows the width of the graphs in Fig. 2 (without lowering their peak heights), thereby reducing the radius of the zone of binding for BCR and forcing the BCR/Ag complexes into a smaller area. BCR/Ag complexes thus form closer to the center than LFA-1/ICAM-1 complexes, resulting in a concentric pattern with BCR/Ag complexes on the inside and LFA-1/ICAM-1 complexes on the outside. If the bond stiffness is sufficiently high for a particular BCR affinity value, the ring of BCR/Ag complexes will compress into a cluster, resulting in a synapse. With increasing BCR affinity, it takes increasingly longer for the BCR/Ag complexes to collect into a cluster (since the dissociation

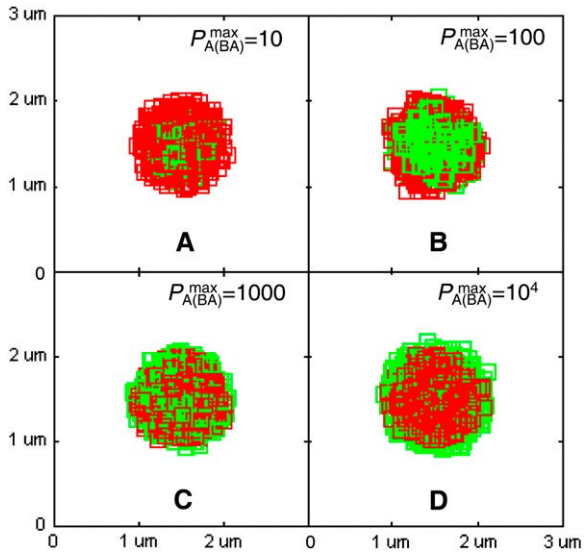

FIGURE 4 Effect of varying BCR affinity ($P^{max}_{A(BA)}$) on synapse formation. BCR/Ag complexes are shown in green, whereas LFA-1/ICAM-1 complexes are shown in red. The complexes are plotted in random order so as to simulate experimental intensity plots as closely as possible. In this set of figures the affinity of BCR was varied from $P^{max}_{A(BA)} = 10$ to $P^{max}_{A(BA)} = 10^4$ ($K_A \approx 10^5$–10^8 M^{-1}). In panel *A* the affinity is too low for synapse formation but in *B* we see that the difference in affinity between BCR and LFA-1 is sufficient to produce a synapse. This is no longer the case in panel *C*, where the affinities are equal, whereas an inverted pattern forms in *D*, where $P^{max}_{A(BA)} > P^{max}_{A(LI)}$. These images were taken after $T = 10^5$ time steps (100 s) with $P^{max}_{A(LI)} = 1000$ ($K_A \approx 10^7$ M^{-1}), $A_0 = I_0 = 2000$ molecules, $\kappa_{BA} = \kappa_{LI} = 40$ μN/m, $z_{eq(BA)} = z_{eq(LI)} = 42$ nm, $p_{diff(F)} = 1$, $p_{diff(C)} = 0.1$, $P^{max}_{on(BA)} = P^{max}_{on(LI)} = 0.1$, $P^{min}_{off(BA)} = 0.01 - 10^{-5}$, and $P^{min}_{off(LI)} = 10^{-4}$.

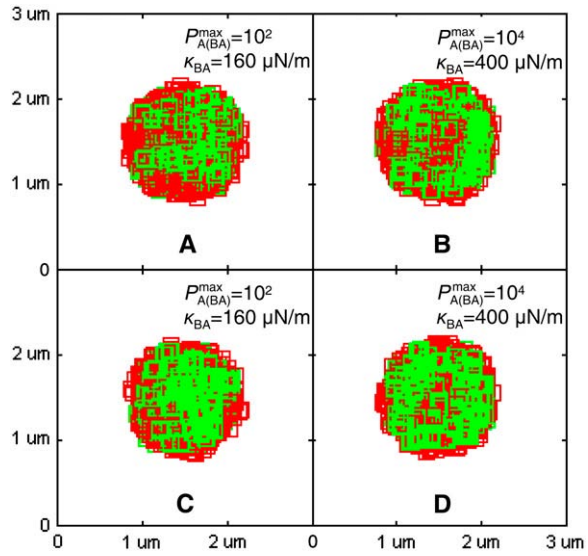

FIGURE 5 Effect of membrane deformation on synapse formation. In panels *A* and *B* no synapse pattern is observed to form when LFA-1 is in a high-affinity state from the start, both for (*A*) low BCR affinity and (*B*) high BCR affinity and high BCR/Ag bond stiffness. In panel *C*, by contrast, we observe a synapse at low BCR affinity ($K_A \approx 10^6$ M^{-1}) provided LFA-1 is initially in a low affinity state and switches to the high-affinity state after $t \sim$ 30 s (also provided $\kappa_{BA} = 160$ μN/m). In panel *D* we see that this mechanism no longer generates a canonical synapse at high BCR affinity ($K_A \geq 10^8$ M^{-1}), even when BCR/Ag bond stiffness is 10-fold greater than that of LFA-1/ICAM-1 ($\kappa_{BA} = 400$ μN/m). These images were taken after $T = 10^5$ time steps (100 s) with $P^{max}_{A(LI)} = 1000$ ($K_A \approx 10^7$ M^{-1}), $A_0 = I_0 =$ 2000 molecules, $\kappa_{LI} = 40$ μN/m, $z_{eq(BA)} = z_{eq(LI)} = 42$ nm, $p_{diff(F)} = 1$ and $p_{diff(C)} = 0.1$, $M \sim 10^{-12}$ m^4/Js, $\gamma = 24$ μN/m, and $\beta = 5 \times 10^{-20}$ J.

probability decreases), and thus a stiffer bond is needed to produce a synapse.

Significant membrane deformation

Synapses cannot form due to affinity differences in the absence of a shift in LFA-1 affinity

No synapses are observed to form by the affinity-dependent mechanism when significant membrane deformation is allowed to take place. At low BCR affinity ($K_A = 10^6$ M^{-1}), the pattern formed is barely recognizable as a synapse, as can be seen in Fig. 5 *A*. The BCR/Ag are not arranged in a compact cluster and the center of the contact region moreover contains large gaps filled by LFA-1/ICAM-1 complexes. At high BCR affinity ($K_A \geq 10^8$ M^{-1}) the BCR/Ag complexes are distributed in a ring at the outer edge of the region where binding is possible, even for relatively high BCR/Ag bond stiffness ($\kappa_{BA} = 400$ μN/m), as can be seen in Fig. 5 *B*.

These results indicate that membrane deformation has a significant and detrimental effect on synapse formation. The explanation for this can be seen in Fig. 6, where we see that as a result of receptor-ligand binding, the membrane separation distance at the zone of binding achieves a uniform value approximately equal to the equilibrium bond length of BCR/Ag and LFA-1/ICAM-1 complexes (~42 nm). The effect of membrane curvature, which previously was crucial to synapse formation by allowing the BCR/Ag complexes to collect into a cluster at a faster rate than LFA-1/ICAM-1 complexes (when BCR affinity was less than LFA-1 affinity) is now entirely negated. As the membrane separation distance in the contact region assumes this uniform value rather rapidly ($t \sim 2000$ time steps; Fig. 6), the initial ring of BCR/Ag complexes never compresses into a compact central cluster, producing the pattern in Fig. 5 *A*. The uniform membrane separation distance in the contact region also negates the previously crucial effect of BCR/Ag bond stiffness at high affinity, as it makes differences in bond stiffness irrelevant. BCR/Ag complexes can thus form at the outer edge of the zone of binding, generating the image seen in Fig. 5 *B*.

A shift in LFA-1 affinity can drive synapse formation

It recently has been hypothesized that LFA-1 on the B-cell surface is initially in a low affinity state before contact with the APC, and that it changes conformation to a high-affinity state after outside-in signaling following BCR activation upon antigen ligation (6,7,9). Our model shows it is possible for synapses to form when significant membrane deformation occurs only when the affinity and stiffness-dependent mechanism is combined with a shift in the affinity of LFA-1 from

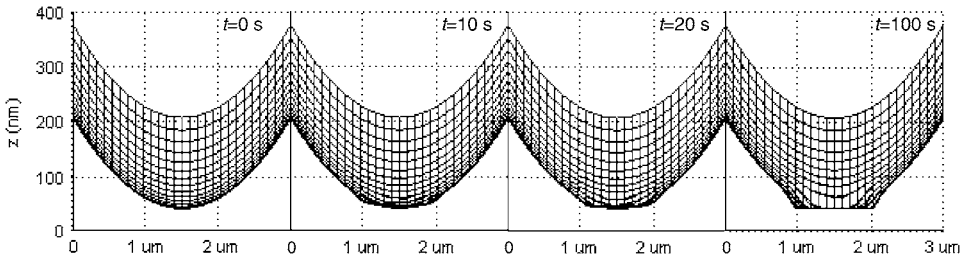

FIGURE 6 Cross-sectional view of the time evolution of membrane shape as a result of receptor-ligand binding. Already by $t = 20$ s, we can see that the membrane separation distance center of the contact zone has more or less attained a uniform value of $z \sim 40$ nm. This image sequence was obtained with $P_{A(BA)} = 100$ ($K_A \approx 10^6$ M^{-1}), $P_{A(LI)} = 1000$ ($K_A \approx 10^7$ M^{-1}), $A_0 = I_0 = 2000$ molecules, $\kappa_{BA} = \kappa_{LI} = 40$ μN/m, $z_{eq(BA)} = z_{eq(LI)} = 42$ nm, $p_{diff(F)} = 1$, $p_{diff(C)} = 0.1$, $M \sim 10^{-12}$ m^4/Js, $\gamma = 24$ μN/m, $\beta = 5 \times 10^{-20}$ J.

low to high as a result of BCR/Ag binding. To model the process, we initially set the affinity of LFA-1 to a low value of $K_A \approx 10^4$ M^{-1}, and switch it to the high-affinity value of $K_A = 10^7$ M^{-1} after 30 s have elapsed. A similar mechanism of LFA-1 affinity modulation has previously been observed in experimental systems involving immune cell activation (37). In Fig. 5 *C* we see that at low BCR affinity, the coupling of a shift in LFA-1 affinity with increased BCR/Ag bond stiffness can result in the formation of synapses where none formed previously (Fig. 5 *A*). Setting the time at which the LFA-1 affinity shift occurs to $t > 30$ s did not produce a significant change in results, whereas decreasing it below this threshold essentially negated its effect. At high BCR affinity ($K_A \geq 10^8$ M^{-1}), however, no synapses are observed to form under any circumstances, regardless of BCR/Ag bond stiffness values or LFA-1 affinity shift (Fig. 5 *D*).

Our explanation for synapse formation due to a shift in LFA-1 affinity is as follows: When LFA-1 affinity is initially low, almost all complexes formed are BCR/Ag complexes. Because fewer complexes are formed, the central portion of the membrane deforms more slowly than when BCR/Ag and LFA-1/ICAM-1 complexes form simultaneously. This gives the initial ring of BCR/Ag complexes enough time to compress into a cluster before the membrane separation distance achieves a uniform value. By the time the affinity of LFA-1 is shifted, allowing rapid LFA-1/ICAM-1 binding, the center of the contact zone is already occupied by the BCR/Ag complexes, so that the LFA-1/ICAM-1 complexes cannot achieve numerical superiority in the center but do so at the periphery, generating a synapse pattern such as in Fig. 5 *C*. As BCR affinity increases above $K_A = 10^7$ M^{-1}, the faster rate of BCR/Ag complex formation results in faster membrane deformation and hence it becomes increasingly difficult for synapses to form (Fig. 5 *D*). This suggests that yet another mechanism must be responsible for synapse formation at high BCR affinity when significant membrane deformation occurs.

Importance of molecular size and diffusion on synapse formation

Though B-cell synapse formation experiments to date mostly consider antigen loaded onto immune complexes (5–7), which results in BCR/Ag complexes of length comparable to LFA-1/ICAM-1 complexes, the possibility that the equilibrium length of the BCR/Ag complexes can vary in vivo and can be equal to its minimum theoretical value ($z_{eq(BA)} = 22$ nm) cannot be ruled out. In our simulations, we find that setting $z_{eq(BA)} = 22$ nm enhances the affinity and signaling-mediated synapse formation mechanisms outlined above in all cases. At the low end of BCR affinity ($K_A < 10^8$ M^{-1}) in particular, the difference in length is sufficient to result in synapses without a difference in bond stiffness or a shift in LFA-1 affinity. Synapses formed with $z_{eq(BA)} = 22$ nm are also larger than with $z_{eq(BA)} = 42$ nm, ~ 1.5 μm in diameter instead of ~ 1 μm.

Throughout our investigations we also observed that synapses only formed when complex diffusivity was lower than free molecule diffusivity by at least an order of magnitude (i.e., $p_{diff(C)} = 0.1$ and $p_{diff(F)} = 1$). This applied regardless of the synapse formation mechanism (affinity and stiffness-dependent or LFA-1 affinity shift-dependent) or membrane deformation regime. Our explanation is that as the diffusivity of the molecular complexes increases, they become more likely to diffuse away from the zone of binding and eventually dissociate, resulting in less ordered and stable patterns. If the molecular complexes are as mobile as free molecules, the synapse will never form as entropic forces will win over free energy gain obtained from the ordered synapse pattern. Thus an order-of-magnitude difference between complex and free molecule diffusivity is needed for synapses to form in all cases. This is consistent with recent studies that show that the mobility of membrane proteins is strongly dependent on size (38–40), and in our simulations the difference in size between free monomeric molecules and BCR/Ag_2 complexes is significant.

Effect of BCR bivalence

Throughout our simulations we have simulated BCR as a bivalent molecule, and it is of interest to compare these results with those obtained when BCR is simulated as a monovalent molecule. The most immediate difference is that fewer BCR/Ag complexes form with monovalent BCR, as the number of binding sites for antigen is essentially cut by half. This results in less dense BCR/Ag clusters and thus a lower probability of

forming a synapse. For instance, the minimum BCR/Ag bond stiffness needed for synapse formation with monovalent BCR is roughly twice that needed with bivalent BCR.

Significantly, it is virtually impossible for synapses to form with monovalent BCR when membrane deformation is included in our model, no matter the BCR/Ag bond stiffness value or whether a shift in LFA-1 affinity occurs. At the low end of the BCR affinity range it is possible to obtain synapses only with both very stiff BCR/Ag bond values (at least an order of magnitude greater than LFA-1/ICAM-1) and a shift in LFA-1 affinity, whereas at the high end of the BCR affinity range no synapses form under any circumstances. Finally, an additional difference is that as a monovalent BCR molecule occupies only one node and can bind only a single antigen molecule, it is more mobile than a bivalent BCR molecule and hence synapse formation requires that $p_{\mathrm{diff(C)}}$ be at least two orders of magnitude lower than $p_{\mathrm{diff(F)}}$ in all cases.

DISCUSSION

Stochastic simulation of B-cell synapse formation reveals that an affinity-dependent mechanism appears sufficient to drive synapse formation in the absence of membrane deformation. When intrinsic BCR affinity is lower than LFA-1 affinity by an order of magnitude, synapses can form solely due to the difference in affinity. When intrinsic BCR affinity is higher than LFA-1 affinity, it is necessary for BCR/Ag bonds to be stiffer than LFA-1/ICAM-1 bonds in order for synapses to form. While we have not found literature values for BCR/Ag bond stiffness, our results indicate that the minimum necessary difference in bond stiffness between the two species is well within an order of magnitude (fourfold at most). Given the wide variety of antigens a B cell can encounter, we hypothesize that the requirement on BCR/Ag bond stiffness is not particularly severe and is likely to be met in many cases, particularly when considering that the intrinsic affinity of BCR for antigen ranges across five orders of magnitude. With the addition of significant membrane deformation, differences in affinity and bond stiffness are not sufficient to drive synapse formation and an additional mechanism, in the form of a signaling-driven shift in the affinity of LFA-1 is necessary. Even with a shift in LFA-1 affinity, however, synapses only form at the low end of BCR affinity, with no synapses observed above $K_{\mathrm{A}} = 10^7\ \mathrm{M}^{-1}$.

Based on our model's results, we propose the following scenario as the most probable mechanism of synapse formation in B cells. As the B cell and APC approach each other, the LFA-1 is in a low affinity state, so that binding begins when the two cells are close enough for a BCR molecule to bind to an antigen molecule. BCR binding to antigen also initiates a signaling cascade directing LFA-1 to change conformation so that it can bind ICAM-1 with high affinity. BCR molecules from the periphery drift into the zone where binding is possible, whereupon they either bind to antigen and form a complex, or eventually drift back out to the periphery again. Because molecular complexes are considerably less mobile than free molecules, they tend to stay where they form, at the edges of the zone of binding, producing a ring-like pattern. This ring becomes more cluster-like over time as some complexes break up and their constituent molecules drift toward the center of the contact zone where they are more likely to bind another molecule. During this process the B-cell membrane deforms to accommodate the BCR/Ag complexes at their equilibrium bond length. After ~30 s have passed, enough LFA-1 molecules have shifted to the high-affinity state so that LFA-1/ICAM-1 binding becomes significant, accelerating membrane deformation and resulting in uniform membrane separation distance at the center of the contact zone. The head start in binding of the BCR, combined with the potentially higher bond stiffness of the BCR/Ag bond, results in BCR/Ag complexes being numerically dominant at the center of the contact zone. The more flexible LFA-1/ICAM-1 bonds are more numerous at the outer part of the contact zone, producing the canonical immunological synapse pattern. At the high end of BCR affinity ($K_{\mathrm{A}} \geq 10^8\ \mathrm{M}^{-1}$), the rate of membrane deformation due to BCR/Ag complex formation is so high that the shift in LFA-1 affinity is not sufficient to produce synapses, leading us to speculate on the existence of additional synapse formation mechanisms for high BCR affinity and significant membrane deformation.

Although the B-cell synapse resembles the T-cell synapse in appearance, our model indicates that the mechanisms of synapse formation between T cells and B cells differ substantially. The primary mechanism of synapse formation in T cells is believed to be the active cytoskeletal drive of the TCR/MHCp complexes toward the center coupled with the difference in extracellular domain length between TCR/MHCp and LFA-1/ICAM-1 (11,12,14,18). Our results show that this is clearly not the case in B cells, where differences in extracellular domain length between the species are negligible (6,7,25,26) and synapses can form without cytoskeletal motion of receptors toward the center.

Comparison of our model's result with experimental data shows substantial agreement. With the mechanisms described above, our model predicts synapse formation over the entire range of physiological BCR affinity values ($K_{\mathrm{A}} = 10^6$–$10^{10}\ \mathrm{M}^{-1}$) (6,7). Furthermore, our model does not produce synapses below $K_{\mathrm{A}} = 10^6\ \mathrm{M}^{-1}$, which is in line with experimental results (6,7). The minimum number of antigen molecules needed for a synapse is ~1000 molecules, which corresponds to a concentration of ~100 molecules/$\mu\mathrm{m}^2$, assuming a contact area of ~9 $\mu\mathrm{m}^2$. The size of the synapses predicted by our model is ~1–1.5 μm in diameter, which is comparable to the 1–2-μm diameter of real synapses. The timescale of synapse formation in our model is of the order of 10^5 time steps, which is mapped to physical time by matching the diffusion coefficients in our simulation to those reported in experiments (see Appendix). This yields a 1 ms per time step mapping, which means our model's timescale

of synapse formation corresponds to the experimentally observed timescale of 1–2 min.

As it stands, our model possesses several attributes that make it particularly suitable for modeling B-cell synapse formation. The approach we are using is stochastic and discrete in nature, and hence is suitable for the modeling of situations of low antigen concentration, such as the onset of the immune response. Our model incorporates the bivalent nature of the BCR as well as changes in membrane shape due to receptor-ligand binding. In addition, we use a Monte Carlo scheme that is computationally efficient and can thus carry out an entire set of virtual experiments in a matter of minutes. Furthermore, we present a novel framework for mapping our model's probabilistic parameters into physical quantities and vice versa (see Appendix). Such a framework is notably absent from similar Monte Carlo models developed to study such systems in the past (20) and to the best of our knowledge is the first of its kind. Finally, our model can be easily modified to model a variety of similar cell-cell systems.

Future work will be aimed at making our model increasingly physiological, especially with regards to the modeling of signaling-induced processes. Most important is the investigation of the mechanisms of synapse formation at high BCR affinity when membrane deformation is significant. Another extension of our work could involve further exploration of the precise form of the LFA-1 affinity shift in B cells, about which little is currently known.

One of the main goals of this study is to make predictions about the process of B-cell synapse formation that may be experimentally tested. Accurate measurement of BCR/Ag bond stiffness, complex diffusivity, membrane deformation, and LFA-1 activation kinetics during synapse formation would go a long way toward establishing the validity of our model's predictions. It is our belief the combination of computational modeling and experimental investigations part of an iterative process can lead to a full understanding of the process of immunological synapse formation in B cells and further account for the physiological responses observed during B-cell immune function.

APPENDIX

Because some of the parameters of our model are probabilistic in nature and therefore dimensionless, it is necessary to map them onto physical quantities to be able to physically interpret the results. Two such mappings are necessary: one that maps the probabilistic affinity P_A^{max} to the association constant K_A and one that maps the size of our model's time step to physical time by relating p_{diff} to the physical diffusion coefficient D.

We begin this section with the mapping between P_A and the association constant K_A. To map values of P_A^{max} onto corresponding values of K_A^{max}, we make use of the fact that at kinetic equilibrium, the two-dimensional association constant, $K_{A(2D)}$, can be obtained from the following relation (12,28,31):

$$K_{A(2D)} = \frac{C_{complex}}{C_{free(1)} \times C_{free(2)}} = \frac{N_{complex}}{N_{free(1)} \times N_{free(2)}} \cdot Area \quad (A1)$$

Here C refers to the concentration (molecules/area), $N_{complex}$ is the number of complexes formed at equilibrium, whereas $N_{free(1)}$ and $N_{free(2)}$ refer to the number of free molecules present at equilibrium. To map P_A^{max} to $K_{A(2D)}$, we run our simulation for a particular value of P_A^{max} to obtain $N_{complex}$, $N_{free(1)}$, and $N_{free(2)}$, and calculate $K_{A(2D)}$ from Eq. A1.

The results are shown in Fig. 7, where we see a linear relationship between $K_{A(2D)}$ and P_A^{max} of the form:

$$K_{A(2D)} = (2 \times 10^{-3}\ \mu m^2/\text{molecules}) \times P_A^{max}. \quad (A2)$$

Because the affinity of BCR in the experimental literature is usually given in units of three-dimensional K_A, it also is necessary to convert values of $K_{A(2D)}$ to $K_{A(3D)}$. This is done by first multiplying by the effective confinement length in the manner of Bell (31), for which we use the thickness of cell membrane ($\sim$10 nm). Because $K_{A(3D)}$ is usually given in units of M^{-1}, the second step in the conversion consists of multiplying by the conversion factor $1L = (0.1\ m)^3 = 10^{15}\ \mu m^3$ and multiplying by Avogadro's number ($1\ mol = 6 \times 10^{23}$ molecules). This results in the following relation between P_A^{max} and $K_{A(3D)}$:

$$K_{A(3D)} = \left(\frac{2\times10^{-3}\mu m^2}{\text{molecules}}\right) \times P_A^{max} \times 0.01\ \mu m \times \frac{1\ L}{10^{15}\mu m^3} \times \frac{6\times10^{23}\text{molecules}}{1\ mol} = (10^4 M^{-1}) \times P_A^{max}. \quad (A3)$$

Thus, for example, the reported value of LFA-1 affinity of 3.3 μm^2/molecule (28) approximately maps to $P_{A(LI)}^{max} = 1000$ (using Eq. A2), which in turn corresponds to $K_{A(3D)} = 10^7\ M^{-1}$ (using Eq. A3).

Next, we establish the mapping of our model's timescale to physical time. There are two ways of doing this: One is to match the number of time steps it takes to obtain a synapse in our model to the timescale of synapse formation in experiments, and from there map p_{diff}, p_{on}^{max}, and p_{off}^{min} to their physical counterparts. Another is to match the p_{diff} for which we obtain a synapse in our model to the diffusion D reported in physical experiments, and allow the timescale of our model to emerge naturally from this. Because it appears more sound, we use the latter approach.

As with affinity, we map the probability of diffusion p_{diff} to the diffusion coefficient D by means of direct simulation. In these simulations, we note the location and time of each molecule as it is created. For complexes, this is simply the time and location at which they form, whereas for free molecules this is either their initial location on the lattice and $t = 0$, or if they have been created as a result of a complex dissociating, the location and time at which

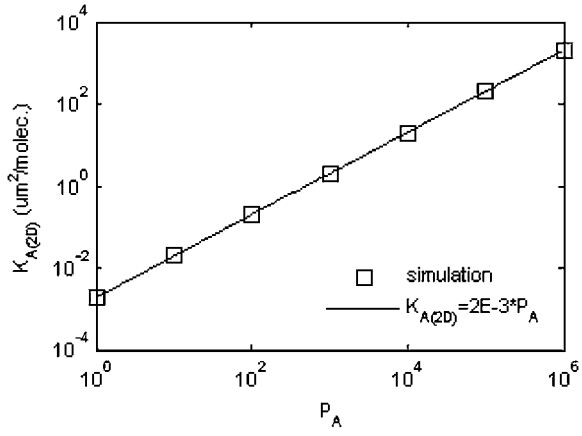

FIGURE 7 Mapping between simulated affinity P_A and $K_{A(2D)}$. The relationship is perfectly linear, with order-of-magnitude increases in P_A corresponding to order of magnitude increases in $K_{A(2D)}$.

the complex dissociated. At each time step, the square of the distance the molecule has traveled from its location of creation is divided by the number of time steps that molecule has been in existence. This is then averaged over all the molecules of that particular type to obtain the simulation diffusion coefficient, D_{sim}, at that particular time step. Thus we have:

$$D_{sim} = \frac{\sum_{i=1}^{N} \frac{(x_{curr} - x_o)^2 + (y_{curr} - y_o)^2}{(t_{curr} - t_o)}}{N}. \quad (A4)$$

We then run the simulation for a particular value of p_{diff} to obtain a time plot of the value of D_{sim} in the manner of Fig. 8. From the figure, we see that a probability of diffusion $p_{diff} = 1$ corresponds to a value of D_{sim} in the range of 0.1–1 (nodal spacings)^2/time step. We then multiply by the appropriate conversion factor to convert the length in nodes to physical length:

$$1.0\frac{(\text{nodal spacings})^2}{\text{time step}} \times \frac{(0.01\,\mu\text{m})^2}{(1\,\text{nodal spacing})^2} = 10^{-4}\frac{\mu\text{m}^2}{\text{time step}}. \quad (A5)$$

We now match this value to that of diffusion coefficient in synapse experiments found in the literature to obtain the physical length of time of one of our model's time steps. The literature value of the diffusion coefficient in synapse experiments of $\sim$0.1 μm^2/s indicates that a single time step in our model corresponds to 0.001 s, i.e., a 1 ms per time step mapping. The observed time of synapse formation of $t = 10^5$ time steps in our simulations thus corresponds to 100 s, which agrees rather well with the experimental time of synapse formation of 1–2 min. With this timescale mapping, the diffusion coefficient mapping now becomes:

$$D_{phys} = \frac{(0.01\,\mu\text{m})^2}{(1\,\text{nodal spacing})^2} \times \frac{10^3\,\text{time steps}}{1\,\text{s}} \times D_{sim} = 0.1\frac{\mu\text{m}^2}{\text{s}} \times D_{sim}. \quad (A6)$$

Once we have obtained the timescale mapping, it is straightforward to map p_{off}^{min} to k_{off} through the relation:

$$k_{off} = \frac{10^3\,\text{time steps}}{\text{s}} \times p_{off}^{min}. \quad (A7)$$

Thus, the reported k_{off} for LFA-1 in the literature of 0.1 s^{-1} (29) corresponds to $p_{off(LI)}^{min} = 10^{-4}$. Multiplying Eqs. A3 and A7, we obtain the mapping between p_{on}^{max} and k_{on}:

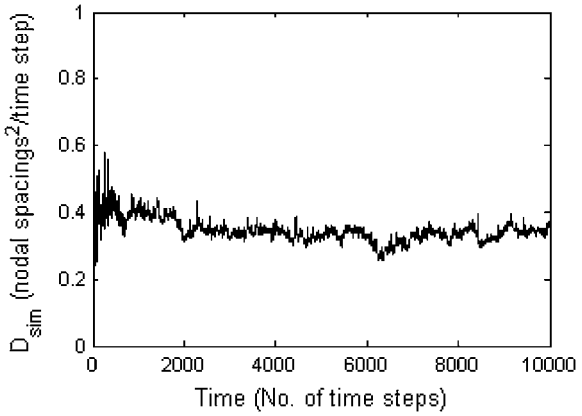

FIGURE 8 Plot of D_{sim} resulting from setting $p_{diff} = 1.0$.

$$k_{on} = (10^7\,\text{M}^{-1}\text{s}^{-1}) \times p_{on}^{max}. \quad (A8)$$

From this, we estimate the measured value of $k_{on} = 2 \times 10^6$ M^{-1}s^{-1} for the HEL line of antigens in Carrasco et al. (6,7) approximately corresponds to a $p_{on}^{max} = 0.1$. Because p_{on}^{max} cannot exceed 1, to simulate values of $k_{on} > 10^7$ M^{-1}s^{-1}, the mapping between p_{diff} and D would have to be changed by matching $p_{diff} = 1$ to a higher D value.

SUPPLEMENTARY MATERIAL

An online supplement to this article can be found by visiting BJ Online at http://www.biophysj.org.

The authors thank Drs. Arup Chakraborty, Rajiv Singh, and Volkmar Heinrich for many insightful discussions over the course of this study. We also acknowledge Dr. Roger Zauel for his valuable help on random number generation.

N.B. acknowledges support from National Institutes of Health grant R01 AI051354. S.S. acknowledges National Institutes of Health grant AI27294.

REFERENCES

1. Wulfing, C., M. D. Sjaastad, and M. M. Davis. 1998. Visualizing the dynamics of T cell activation: intracellular adhesion molecule 1 migrates rapidly to the T cell/B cell interface and acts to sustain calcium levels. *Proc. Natl. Acad. Sci. USA.* 95:6302–6307.
2. Monks, C. R., B. A. Freiberg, H. Kupfer, N. Sciaky, and A. Kupfer. 1998. Three-dimensional segregation of supramolecular activation clusters in T cells. *Nature.* 395:82–86.
3. Grakoui, A., S. K. Bromley, C. Sumen, M. M. Davis, A. S. Shaw, P. M. Allen, and M. L. Dustin. 1999. The immunological synapse: a molecular machine controlling T cell activation. *Science.* 285:221–227.
4. Krummel, M. F., M. D. Sjaastad, C. Wulfing, and M. M. Davis. 2000. Differential clustering of CD4 and CD3ζ during T cell recognition. *Science.* 289:1349–1352.
5. Batista, F. D., D. Iber, and M. S. Neuberger. 2001. B cells acquire antigen from target cells after synapse formation. *Nature.* 411:489–494.
6. Carrasco, Y. R., S. J. Fleire, T. Cameron, M. L. Dustin, and F. D. Batista. 2004. LFA-1/ICAM-1 interaction lowers the threshold of B cell activation by facilitating B cell adhesion and synapse formation. *Immunity.* 20:589–599.
7. Carrasco, Y., and F. D. Batista. 2006. B-cell activation by membrane-bound antigens is facilitated by the interaction of VLA-4 with VCAM-1. *EMBO J.* 25:889–899.
8. Fleire, S. J., J. P. Goldman, Y. R. Carrasco, M. Weber, D. Bray, and F. D. Batista. 2006. B cell ligand discrimination through a spreading and contracting response. *Science.* 312:738–741.
9. Carrasco, Y. R., and F. D. Batista. 2006. B cell recognition of membrane-bound antigen: an exquisite way of sensing ligands. *Curr. Op. Immun.* 18:286–291.
10. Bray, D., M. D. Levin, and C. J. Morton-Firth. 1998. Receptor clustering as a cellular mechanism to control sensitivity. *Nature.* 393: 85–88.
11. Qi, S. Y., J. T. Groves, and A. K. Chakraborty. 2001. Synaptic pattern formation during cellular recognition. *Proc. Natl. Acad. Sci. USA.* 98: 6548–6553.
12. Burroughs, N. J., and C. Wülfing. 2002. Differential segregation in a cell-cell contact interface: The dynamics of the immunological synapse. *Biophys. J.* 83:1784–1796.
13. Lee, K. H., A. R. Dinner, C. Tu, G. Campi, S. Raychaudhri, R. Varma, T. N. Sims, W. R. Burack, H. Wu, J. Wang, O. Kanagawa, M. Markiewicz, et al. 2003. The immunological synapse balances T cell receptor signaling and degradation. *Science.* 302:1218–1222.

14. Lee, S. J. E., Y. Hori, J. T. Groves, M. L. Dustin, and A. K. Chakraborty. 2002. Correlation of a dynamic model for immunological synapse formation with effector functions: two pathways to synapse formation. *Trends Immunol.* 23:492–502.

15. Lee, S. J. E., Y. Hori, and A. K. Chakraborty. 2003. Low T cell receptor expression and thermal fluctuations contribute to formation of dynamic multifocal synapses in thymocytes. *Proc. Natl. Acad. Sci. USA.* 100:4383–4388.

16. Raychaudhuri, S., A. K. Chakraborty, and M. Kardar. 2003. Effective membrane model of the immunological synapse. *Phys. Rev. Lett.* 91: 208101.

17. Coombs, D., M. Dembo, C. Wofsy, and B. Goldstein. 2004. Equilibrium thermodynamics of cell-cell adhesion mediated by multiple ligand-receptor pairs. *Biophys. J.* 86:1408–1423.

18. Weikl, T. R., and R. Lipowsky. 2004. Pattern formation during T-cell adhesion. *Biophys. J.* 87:3665–3678.

19. Iber, D. 2005. Formation of the B-cell synapse: retention or recruitment? *Cell. Mol. Life Sci.* 62:206–213.

20. Goldstein, B., J. R. Faeder, and W. S. Hlavacek. 2004. Mathematical and computational models of immune-receptor signaling. *Nature Rev. Immunol.* 4:445–456.

21. Hammer, D., and S. Apte. 1991. Simulation of cell rolling and adhesion of surfaces in shear flow: general results and analysis of selectin-mediated neutrophil adhesion. *Biophys. J.* 63:35–57.

22. Mahama, P. A., and J. J. Linderman. 1995. Monte Carlo simulations of membrane signal transduction events: effect of receptor blockers on G-protein activation. *Ann. Biomed. Eng.* 23:299–307.

23. Van Kampen, N. G. 2001. Stochastic Processes in Physics and Chemistry. Elsevier, Amsterdam, The Netherlands.

24. Chakraborty, A. K., M. L. Dustin, and A. S. Shaw. 2003. *In silico* models for cellular and molecular immunology: successes, promises, and challenges. *Nat. Immunol.* 4:933–936.

25. Alberts, B., A. Johnson, J. Lewis, M. Raff, D. Bray, K. Hopkin, K. Roberts, and P. Walters. 2003. Essential Cell Biology, 2nd ed. Garland Science, London.

26. Alberts, B., A. Johnson, J. Lewis, M. Raff, K. Roberts, and P. Walter. 2002. Molecular Biology of the Cell, 4th Ed. Garland Science, London, UK.

27. Dembo, M., T. C. Torney, K. Saxman, and D. Hammer. 1988. The reaction-limited kinetics of membrane-to-surface adhesion and detachment. *Proc. R. Soc. Lond. B Biol. Sci.* 234:55–83.

28. Lauffenburger, D. A., and J. J. Linderman. 1993. Models for Binding, Trafficking and Signaling. Oxford University Press, Oxford, UK.

29. Tominaga, Y., Y. Kita, A. Satoh, S. Asai, K. Kato, K. Ishikawa, T. Horiuchi, and T. Takashi. 1998. Expression of a soluble form of LFA-1 and demonstration of its binding activity with ICAM-1. *J. Immunol. Meth.* 212:61–68.

30. Favier, B., N. J. Burroughs, L. Weddeburn, and S. Valitutti. 2001. T cell antigen receptor dynamics on the surface of living cells. *Int. Immunol.* 13:1525–1532.

31. Bell, G. I. 1983. Cell-cell adhesion in the immune system. *Immunol. Today.* 4:237–240.

32. Lanzavecchia, A. 1985. Antigen-specific interaction between T and B cells. *Nature.* 314:537–539.

33. Batista, F. D., and M. S. Neuberger. 1998. Affinity dependence of the B-cell response to antigen: a threshold, a ceiling, and the importance of off-rate. *Immunity.* 8:751–759.

34. Kouskoff, V., S. Famiglietti, G. Lacaud, P. Lang, J. E. Rider, B. K. Kay, J. C. Cambier, and D. Nemazee. 1998. Antigens varying in affinity for the B cell receptor induce differential B lymphocyte responses. *J. Exp. Med.* 188:1453–1464.

35. Shih, T. A., E. Meffre, M. Roederer, and M. C. Nussenzweig. 2002. Role of antigen receptor affinity in T cell-independent antibody responses in vivo. *Nat. Immunol.* 3:399–406.

36. Shih, T. A., E. Meffre, M. Roederer, and M. C. Nussenzweig. 2002. Role of BCR affinity in T cell dependent responses in vivo. *Nat. Immunol.* 3:570–575.

37. Lum, A. F. H., C. E. Green, G. R. Lee, D. E. Staunton, and S. I. Simon. 2002. Dynamic regulation of LFA-1 activation and neutrophil arrest on intercellular adhesion molecule 1 (ICAM-1) in shear flow. *J. Biol. Chem.* 277:20660–20670.

38. Kahya, N., D. A. Wiersma, B. Poolman, and D. Hoekstra. 2002. Spatial reorganization of bacteriorhodopsin in model membranes: light induced changes. *J. Biol. Chem.* 277:39304–39311.

39. Lee, C. C., and O. N. Petersen. 2003. The lateral diffusion of selectively aggregated peptides in giant unilamellar vesicles. *Biophys. J.* 84:1756–1764.

40. Gambin, Y., R. Lopez-Esparza, M. Reffay, E. Sierecki, N. S. Gov, M. Genest, R. S. Hodges, and W. Urbach. 2005. Lateral mobility of proteins in liquid membranes revisited. *Proc. Natl. Acad. Sci. USA.* 103:2098–2102.